

Figure 8.14. Comparative study for multigrid schemes using various smoothing operators for  $41 \times 41$  (finest) grid.

convergence rates for the SOR iteration procedure using finer grids. Hence, Ghia and coworkers<sup>9</sup> employed the multigrid technique for convergence acceleration. The emphasis here is not so much on the overall results as on the efficient solution of the Neumann BVP encountered in this problem.

Figure 8.13 shows the convergence history for  $p$  using a total of four grid levels, with a  $41 \times 41$  finest grid, for the curved polar duct with grid clustering near the walls. The smoothing operator used in the MG technique was the Gauss-Seidel iteration. The

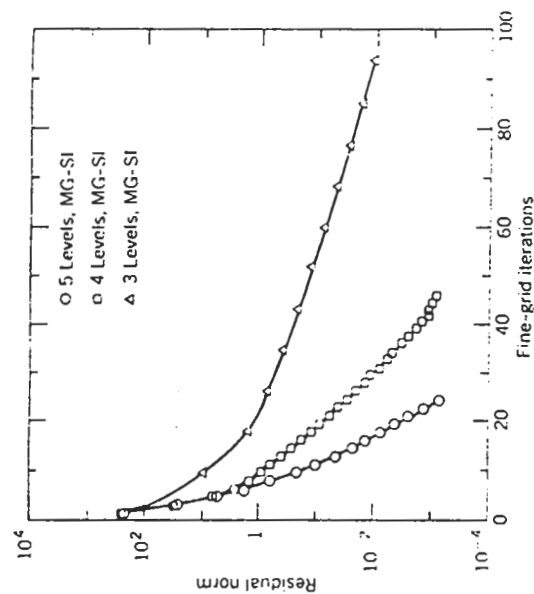


Figure 8.15. Convergence history for Neumann-Poisson problem for  $81 \times 81$  grid.

corresponding convergence histories for the three-level MG procedure as well as the single grid with the optimum SOR method are also included. The four-level MG-GS procedure leads to a threefold reduction in the number of iterations compared to the SG-SOR scheme.

The effect of the smoothing operator employed in the MG procedure on the overall convergence rate is presented in Fig. 8.14, which shows the convergence history for  $p$  for the MG-GS, MG-ADI, and MG-SI schemes. The SI smoothing provides the fastest convergence, while GS smoothing leads to the slowest convergence of the MG scheme. Therefore, for a further refinement of the finest grid to  $81 \times 81$  points, the Neumann problem was solved using the MG-SI scheme; convergence for this grid is obtained in the equivalent of only 25 finest-grid iterations (Fig. 8.15).

#### 8.5.4 Results for Driven-Cavity Problem

The laminar incompressible flow in a square cavity whose top wall moves with a uniform velocity in its own plane is commonly used as a model problem for testing and evaluating numerical techniques, in spite of the singularities at two of its corners. The nomenclature for this problem is shown in Fig. 8.16. For moderately high Reynolds number values, published results are available for this problem from a number of sources (e.g., Refs. 20, 40, and 41), using a variety of solution procedures, including an attempt to analytically extract the corner singularities from the dependent variables of the problem.<sup>42</sup> Some accurate results are now available for high Re also (e.g., Refs. 26 and 43-45). In view of the extensive use of the driven-cavity flow as a model problem, Tables 8.4 and 8.5 list, for ready reference, the numerical values for velocities along lines passing through the geometric center of the cavity.<sup>26</sup> Only typical points, rather than the entire set of computational points, are listed. In particular, the points of local maxima and minima are included for all Re values; these values are underscored. The

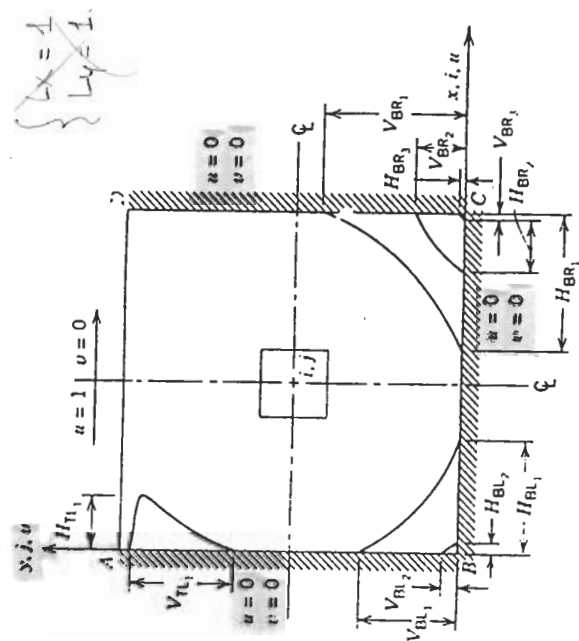


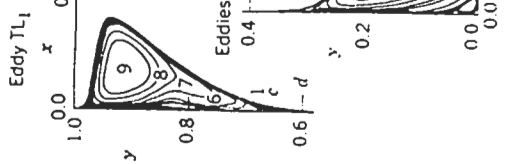
Figure 8.16. Nomenclature of driven square-cavity problem.

TABLE 8.4. Results for  $u$  Velocity along Vertical Line through Geometric Center of Cavity

Pt. No.	$y$	Reynolds Number, $Re$										$Re$
		100	400	1000	3200	5000	7500	10,000	10,000	10,000	10,000	
129	1.00000	1.00000	1.00000	1.00000	1.00000	1.00000	1.00000	1.00000	1.00000	1.00000	1.00000	
126	0.9766	0.84123	0.75837	0.65928	0.53236	0.48223	0.47244	0.47221	0.47221	0.47221	0.47221	
125	0.9688	0.78871	0.68439	0.57492	0.46120	0.47048	0.47048	0.47048	0.47048	0.47048	0.47048	
124	0.9609	0.73722	0.61756	0.51117	0.46547	0.45992	0.47323	0.48070	0.48070	0.48070	0.48070	
123	0.9531	0.68717	0.55892	0.46604	0.46101	0.46036	0.47167	0.47804	0.47804	0.47804	0.47804	
110	0.8516	0.23151	0.29093	0.33304	0.34682	0.33556	0.34228	0.34635	0.34635	0.34635	0.34635	
95	0.7344	0.00332	0.16256	0.18719	0.19791	0.20087	0.20591	0.20673	0.20673	0.20673	0.20673	
80	0.6172	-0.13641	0.02135	0.05702	0.07156	0.08183	0.08342	0.08344	0.08344	0.08344	0.08344	
65	0.5000	-0.20581	-0.11477	-0.06080	-0.04272	-0.03039	-0.03800	-0.03111	-0.03111	-0.03111	-0.03111	
59	0.4531	-0.21090	-0.17119	-0.10648	-0.06636	-0.07404	-0.07503	-0.07540	-0.07540	-0.07540	-0.07540	
37	0.2813	-0.15662	-0.32726	-0.27805	0.34427	-0.22855	-0.23176	-0.23186	-0.23186	-0.23186	-0.23186	
23	0.1719	-0.10150	-0.24299	-0.38289	-0.34327	-0.33050	-0.32393	-0.32709	-0.32709	-0.32709	-0.32709	
14	0.1016	-0.06434	-0.14612	-0.29730	-0.41937	-0.40435	-0.38324	-0.38000	-0.38000	-0.38000	-0.38000	
10	0.0703	-0.04775	-0.10338	-0.22220	-0.37827	-0.43643	-0.43025	-0.41657	-0.41657	-0.41657	-0.41657	
9	0.0625	-0.04192	-0.09266	-0.20196	-0.35344	-0.42901	-0.43590	-0.42537	-0.42537	-0.42537	-0.42537	
8	0.0547	-0.03717	-0.08186	-0.18109	-0.32407	-0.41165	-0.43154	-0.42735	-0.42735	-0.42735	-0.42735	
1	0.0000	0.00000	0.00000	0.00000	0.00000	0.00000	0.00000	0.00000	0.00000	0.00000	0.00000	

TABLE 8.5. Results for  $v$  Velocity along Horizontal Line through Geometric Center of Cavity

Pt. No.	$x$	Reynolds Number, $Re$									
		100	400	1000	3200	5000	7500	10,000	10,000	10,000	10,000
129	1.0000	0.00000	0.00000	0.00000	0.00000	0.00000	0.00000	0.00000	0.00000	0.00000	0.00000
125	0.9688	-0.05906	-0.12146	-0.21383	-0.39117	-0.49774	-0.51858	-0.54102	-0.54102	-0.54102	-0.54102
124	0.9609	-0.07391	-0.15663	-0.27669	-0.47425	-0.55069	-0.55216	-0.52987	-0.52987	-0.52987	-0.52987
123	0.9531	-0.08864	-0.19254	-0.33714	-0.52357	-0.55408	-0.52147	-0.49099	-0.49099	-0.49099	-0.49099
122	0.9453	-0.10313	-0.22847	-0.39188	-0.54053	-0.52876	-0.48990	-0.45863	-0.45863	-0.45863	-0.45863
117	0.9063	-0.16914	-0.23827	-0.51550	-0.44307	-0.41442	-0.41050	-0.41496	-0.41496	-0.41496	-0.41496
111	0.8594	-0.22445	-0.44993	-0.42665	-0.37401	-0.36214	-0.36213	-0.36737	-0.36737	-0.36737	-0.36737
104	0.8047	-0.24533	-0.38598	-0.31966	-0.31184	-0.30018	-0.30448	-0.30719	-0.30719	-0.30719	-0.30719
65	0.5000	0.05454	0.05186	0.02526	0.00999	0.00945	0.00824	0.00831	0.00831	0.00831	0.00831
31	0.2344	0.17527	0.30174	0.32235	0.28188	0.27280	0.27348	0.27224	0.27224	0.27224	0.27224
30	0.2266	0.17507	0.30203	0.33075	0.29030	0.28066	0.28117	0.28003	0.28003	0.28003	0.28003
21	0.1563	0.16077	0.28124	0.37095	0.37119	0.35368	0.35060	0.35070	0.35070	0.35070	0.35070
13	0.0938	0.12317	0.22965	0.32627	0.42768	0.42951	0.41824	0.41487	0.41487	0.41487	0.41487
11	0.0781	0.10890	0.20920	0.30353	0.41906	0.43648	0.43564	0.43124	0.43124	0.43124	0.43124
10	0.0703	0.10091	0.19713	0.29012	0.40917	0.43329	0.44030	0.43733	0.43733	0.43733	0.43733
9	0.0625	0.09233	0.18360	0.27485	0.39560	0.42447	0.43979	0.43983	0.43983	0.43983	0.43983
1	0.0000	0.00000	0.00000	0.00000	0.00000	0.00000	0.00000	0.00000	0.00000	0.00000	0.00000

Figure 8.17. Streamline contours in driven cavity.  $Re = 10,000$ , Uniform finest grid ( $257 \times 257$ ).

streamline contours for  $Re = 10,000$  are shown in Fig. 8.17; a magnified view of the various secondary vortices is also included. The values of  $\psi$  along the contours are listed in Table 8.6.

The computational advantage gained by the use of the MG procedure in the computation of Navier-Stokes solutions is illustrated in Fig. 8.18, in terms of the behavior of  $e_M$ , the  $L_2$  norm of the residuals in the discretized governing equations in the finest grid. The results for a single-grid computation with  $h = \frac{1}{128}$  (solid curve) as well as a multigrid calculation with  $h_M = \frac{1}{128}$  and  $M = 6$  (solid and dashed curves) are

TABLE 8.6. Values of Streamline Contours in Fig. 8.17

Contour Letter	Stream function	
	Value of $\psi$	Contour Number
a	$-1.0 \times 10^{-10}$	0
b	$-1.0 \times 10^{-7}$	1
c	$-1.0 \times 10^{-5}$	2
d	$-1.0 \times 10^{-4}$	3
e	-0.0100	4
f	-0.0300	5
g	-0.0500	6
h	-0.0700	7
i	-0.0900	8
j	-0.1000	9
k	-0.1100	10
l	-0.1150	
m	-0.1175	